

Small-signal modeling, stability analysis, and controller design of grid-friendly power converters with virtual inertia and grid-forming capability

Deng, Han; Fang, Jingyang; Yu, Jiale; Tang, Yi; Debusschere, Vincent

2019

Deng, H., Fang, J., Yu, J., Tang, Y., & Debusschere, V. (2019). Small-signal modeling, stability analysis, and controller design of grid-friendly power converters with virtual inertia and grid-forming capability. IEEE Energy Conversion Congress and Exposition (ECCE).

<https://hdl.handle.net/10356/92194>

© 2019 IEEE. Personal use of this material is permitted. Permission from IEEE must be obtained for all other uses, in any current or future media, including reprinting/republishing this material for advertising or promotional purposes, creating new collective works, for resale or redistribution to servers or lists, or reuse of any copyrighted component of this work in other works.

Downloaded on 09 Apr 2024 17:15:48 SGT

Small-Signal Modeling, Stability Analysis, and Controller Design of Grid-Friendly Power Converters with Virtual Inertia and Grid-Forming Capability

Deng Han
Energy Research Institute @ NTU
ERI@N
Interdisciplinary Graduate Programme
Nanyang Technological University
Singapore
E-mail: han017@e.ntu.edu.sg

Jingyang Fang, Jiale Yu, Yi Tang
School of Electrical and Electronic
Engineering
Nanyang Technological University
Singapore
E-mail: jfang006@e.ntu.edu.sg,
yu0003le@e.ntu.edu.sg,
yitang@ntu.edu.sg

Vincent Debusschere
Univ. Grenoble Alpes, CNRS
Grenoble INP*, G2Elab,
38000 Grenoble
France
E-mail:
vincent.debusschere@grenoble-inp.fr

Abstract— Distributed virtual inertia provided by grid-friendly power converters is emerging as an effective way for inertia enhancement and frequency regulation improvement in more-electronics power systems. However, most existing methods attempt to generate distributed virtual inertia by grid-following power converters. As compared with conventional grid-feeding power converters, grid-forming power converters, i.e. the ones controlled as ac voltage sources, are more promising owing to their capabilities of voltage and frequency regulation. As such, this paper explores the possibility of inertia emulation by grid-forming power converters. Through the stability analysis, it is revealed that the instability issue is associated with typical virtual inertia control. Further, a lead-lag compensator is introduced to resolve this issue. To better stabilize the system, a detailed small signal model is derived, and the sensitivity analysis is applied to study the critical poles.

Keywords— virtual inertia, grid-forming power converters, small signal model, stability

I. INTRODUCTION

The ever-increasing penetration level of power electronics-based renewable generation systems reduces the proportion of synchronous generators (SGs) in modern power systems. As a result, the power system inertia mainly contributed by synchronous generators continues to decrease. Further, the lack of inertia translates into poor frequency regulation performances and even grid failures.

As a solution, the concept of distributed virtual inertia provided by grid-friendly power converters has been proposed in the hope of improving the inertia level of more-electronics power systems [1]. From the grid's perspective, grid-friendly power converters can be broadly classified into two types – the grid-feeding ones which are equivalent to ac current sources and the grid-forming ones which are controlled as ac voltage sources[2], i.e. voltage-controlled converters (VCCs). Specifically, grid-feeding power converters simply regulate their output currents or power and follow the grid without regulating the grid voltages. In contrast, grid-forming power converters regulate voltage and frequency directly as SGs do. They allow the seamless transition between grid-tied and standalone operation. The fragile phase-locked loops (PLL) are not necessarily required for a VCC on account of the self-synchronization characteristic of grid-forming converters [3].

VCCs form the power grid, and therefore at least one such converter is required in electronics-based power systems. Nevertheless, previous research works focus more on inertia emulation by grid-following power converters, and the implementation of providing virtual inertia with grid-forming power converters remains to be explored.

The concept of virtual synchronous machines (VSMs) was proposed to emulate the inertia characteristics and the droop mechanisms of SGs with grid-forming converters [4]. This paper reveals that implementing inertia with grid-forming converters may introduce instability issues. The droop mechanism damps the oscillation caused by implementing virtual inertia with grid-forming converters [5], while the droop mechanism will lead to continuous active power outputs when the grid frequency deviates from the nominal value. As a result, the performance of the droop control is limited by the dc-link source capacity. To address the instability issue and better damp the oscillation, an inertia emulation strategy for grid-forming power converters is proposed in this paper. As a solution for the instability issue, a lead-lag compensator is introduced.

Further, a detailed small signal model including the plant model, the current and voltage controllers and the power controllers is further developed. The relationships between the eigenvalues of the small signal model and the system parameters are studied with sensitivity analysis [6]. Based on the sensitivity analysis results, the control parameters are further chosen to make the system more stable.

II. INERTIA EMULATION BY GRID-FORMING POWER CONVERTERS

Fig. 1 shows the system configuration, where the grid-forming power converter is connected to the grid through an *LCL* filter composed of L_{gi} , C_{gf} and L_{gg} , and L_s denotes the line inductance. The dc side of the grid-forming converter is a dc voltage source whose amplitude is v_{dc} . The basic objectives of grid-forming power converters are to regulate the power flow through controlling the amplitude v_{gf_ref} and phase angle δ of v_{gabc} , i.e., the voltage across C_{gf} .

As seen in Fig. 1, the controllers are implemented in the synchronous *dq*-frame. The power controller generates two inputs for the ac voltage controller, namely δ and v_{gf_ref} . Then the output of the voltage controller, i.e. v_{gidq} are transformed

* Institute of Engineering Univ. Grenoble Alpes

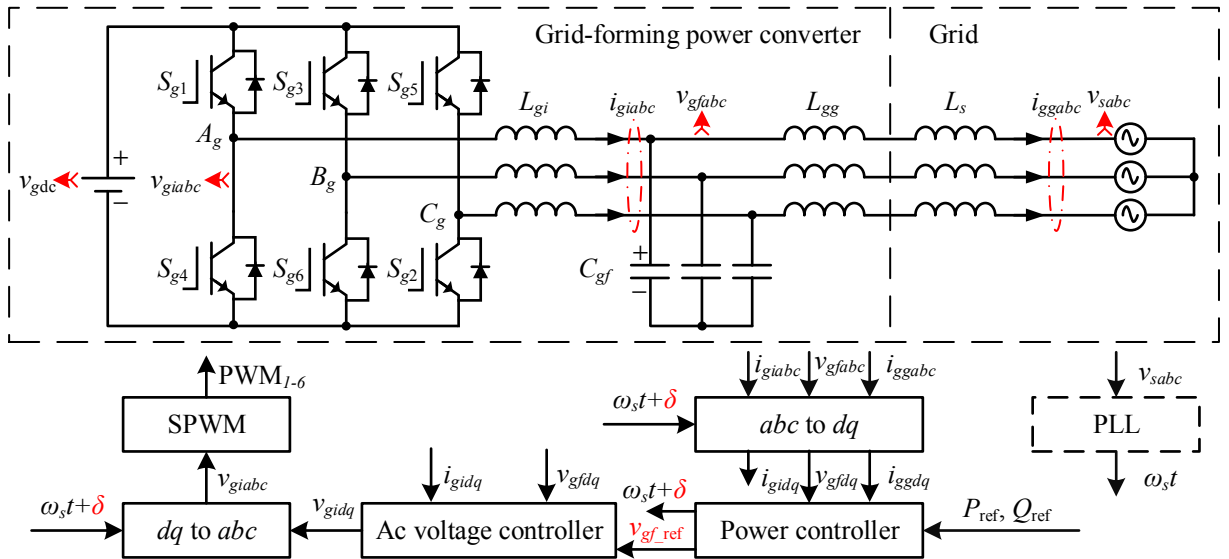


Fig. 1. Schematic diagram of a grid-forming power converter.

from the *dq* frame into the *abc* frame and fed into the pulse width modulator (PWM) to generate gate drive signals for the power switches S_{g1} to S_{g6} .

The current phasor is derived as:

$$\vec{I}_{gg} = \frac{V_{gf} \angle \delta - V_s \angle 0}{jX_T} = \frac{V_{gf} \cos \delta - V_s + jV_{gf} \sin \delta}{jX_T} \quad (1)$$

where V_{gf} and V_s are the converter voltage amplitude and the grid voltage amplitude, respectively, δ is the phase angle difference between the voltage across C_{gf} and the grid voltage, $X_T = j\omega_0(L_{gg} + L_s)$ is the lumped impedance consisting of line impedance and grid side impedance, and ω_0 stands for the nominal grid frequency. Further, the active power P and the reactive power Q injected into the grid can be calculated as follows:

$$P = \text{Re} \left[\frac{3}{2} \vec{V}_{gf} \vec{I}_{gg}^* \right] = \frac{3V_{gf}V_s \sin \delta}{2X_T} \quad (2)$$

$$Q = \text{Im} \left[\frac{3}{2} \vec{V}_{gf} \vec{I}_{gg}^* \right] = \frac{3(V_{gf} - V_s \cos \delta)V_{gf}}{2X_T} \quad (3)$$

Similar to the control of SGs, grid forming converters usually regulate the phase angle δ and voltage amplitude V_{gf} to control the active power P and reactive power Q output, respectively [3]. When the power angle δ is smaller than 0.1 rad, the coupling effect between the active power and reactive power control can be neglected [5], and the active power angle equation can be linearized as

$$\Delta P = \frac{3V_{gf}V_s}{2X_T} \Delta \delta \quad (4)$$

where the prefix Δ refers to the perturbed quantity. According to the well-known swing equation [7]

$$(\Delta P_{m_pu} - \Delta P_{e_pu}) = 2H \frac{d\Delta\omega_{r_pu}}{dt} \quad (5)$$

and the linearized power angle equation (4), a simplified active power control loop for grid-forming power converters with distributed virtual inertia is shown in Fig. 2, where the subscript pu denotes the per unit notation, p_{ref} and p_{g_c} represent the power reference and the converter output

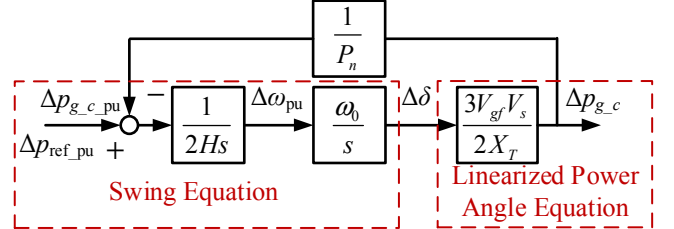


Fig. 2. The simplified active power control loop.

electrical power, ω_0 is the fundamental angular frequency, ω stands for the electrical angular speed, P_n is the nominal power, and H is the inertia constant. To be specific, a larger value of H translates into higher inertia, indicating improved frequency regulation in terms of rate-of-change-of-frequency (RoCoF) and frequency nadir [3].

However, this system is unstable as it has a pair of poles, i.e. $s_{1,2} = \pm j\omega_p = \pm j \sqrt{\frac{3\omega_0 V_{gf} V_s}{4P_n H X_T}}$, on the imaginary axis. To stabilize the system, a lead-lag compensator

$$G_{LL}(s) = \frac{K_f s + \omega_c}{s + \omega_c} \quad (6)$$

is introduced into the power controller, in which ω_c denotes its passband frequency, and K_f is the compensator gain. By selecting the compensator parameters coarsely to make $\omega_p \in (\frac{\omega_c}{K_f}, \omega_c)$, the phase boost can make the system stable, and the lead-lag compensator will not change the steady-state gain of the original controller as $G_{LL}(0) = 1$. As a result, the designed grid-tied VCC is stabilized without introducing droop mechanism, which is restricted by the dc source capacity. Next section will give a detailed model of grid-forming power converters, based on which the stability analysis and stability enhancement method will be carried out. With the sensitivity analysis, the values of ω_c and K_f are adjusted more precisely to make the corresponding poles more left to the imaginary axis.

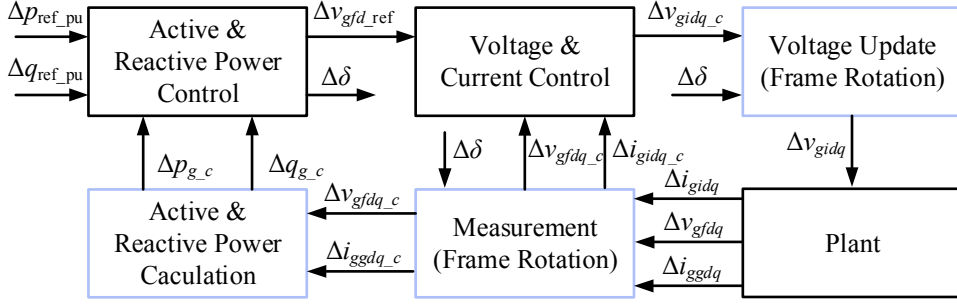


Fig. 3. Small signal model of grid-forming power converters.

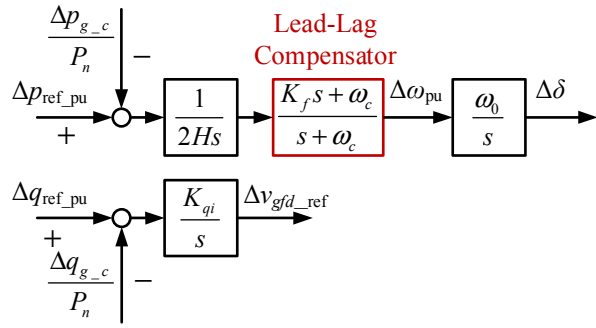


Fig. 4. Control for active and reactive power.

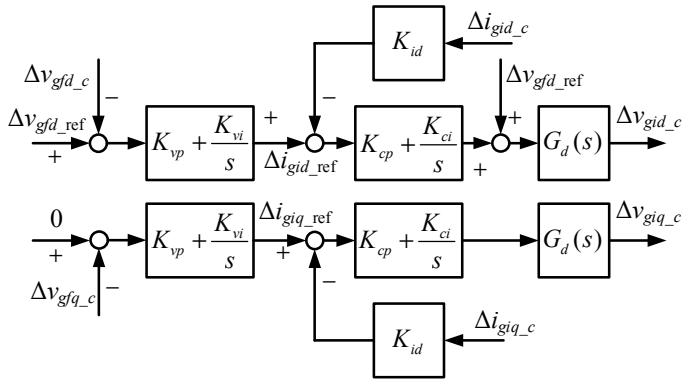


Fig. 5. Control for voltage and current.

III. SMALL SIGNAL MODELING AND SENSITIVITY ANALYSIS

Fig. 3 shows the small signal model of grid-forming power converters, where the subscript dq is used to represent signals in the synchronous dq -frame. Moreover, the signals without the subscript c are in the plant dq -frame, while the subscript c refers to signals in the control dq -frame (note that $v_{sq} = 0$ and $v_{gfp_c} = 0$). The model is mainly divided into 3 parts, namely the active and reactive power control, the voltage and current control, and the plant. Because the control frame leads the plant frame by δ , frame rotations are required for signal transformations.

The models in Fig. 3 are further detailed in Fig. 4 to Fig. 8. Specifically, the active and reactive power control model is shown in Fig. 4, where the proposed lead-lag compensator aims to stabilize the system. Fig. 5 depicts the voltage and current control model, where the current and voltage controllers are implemented as PI controllers, and

$$G_d(s) = e^{-1.5T_s s} \approx \frac{1 - \frac{1.5T_s}{2}s}{1 + \frac{1.5T_s}{2}s} \quad (7)$$

denotes the transfer function of the sampling and PWM delay linearized with Pade approximation, in which T_s is the sampling period of the system. Fig. 6 visualizes the plant model of the system shown in Fig. 1 in the dq frame, Fig. 7 gives the power calculation model, and Fig. 8 illustrates the frame rotation models, where the variables in the upper case are the steady-state values of those in the lower case.

The state space model, i.e.,

$$\dot{\mathbf{x}} = \mathbf{A}\mathbf{x} + \mathbf{B}\mathbf{u} \quad (8)$$

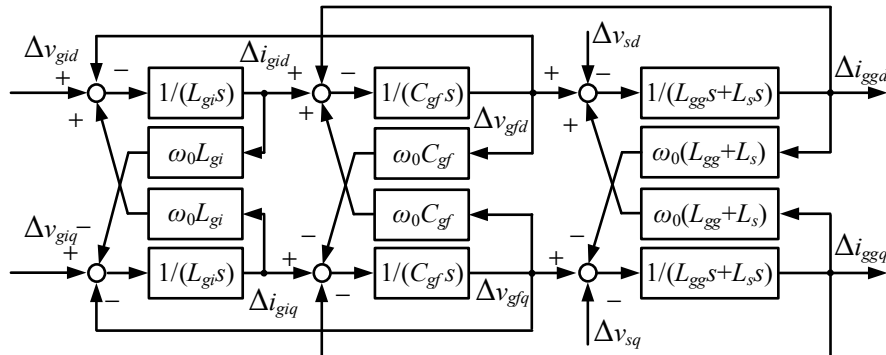


Fig. 6. Plant model.

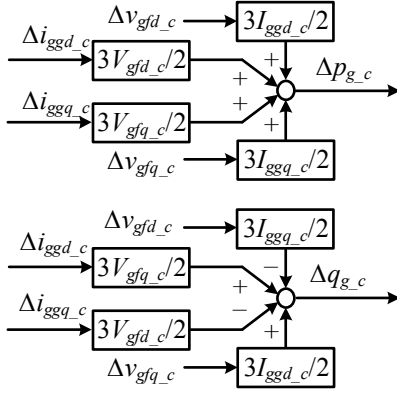


Fig. 7. Power calculation.

is built to combine the models in Fig. 3 together, where \mathbf{u} is the input vector $[\Delta p_{\text{ref_pu}} \Delta q_{\text{ref_pu}} \Delta v_{sd} \Delta v_{sq}]^T$, \mathbf{x} is the state vector $[\Delta x_{pe} \Delta x_{pc} \Delta \delta \Delta x_{pe} \Delta x_{vd} \Delta x_{vq} \Delta x_{cd} \Delta x_{cq} \Delta x_{dd} \Delta x_{dq} \Delta i_{gid} \Delta i_{gq} \Delta v_{gfd} \Delta v_{gq} \Delta i_{gqd} \Delta i_{gqg}]^T$, and \mathbf{A} , \mathbf{B} are shown in the appendix. The input vector \mathbf{u} contains the power references and the grid voltages in the dq frame, and the state vector \mathbf{x} is composed of the states in Fig. 4 to Fig. 6. The eigenvalues of \mathbf{A} are shown in Fig. 9, indicating that the system without the lead-lag compensator (i.e., $K_f = 1$) will be unstable.

To determine the influence of each design parameter on the system stability, the sensitivity analysis is carried out. The following equation describes the sensitivity of the n^{th} eigenvalue to the k^{th} parameter [3]:

$$\frac{\partial \lambda_n}{\partial \rho_k} = \frac{\Phi_n^T \frac{\partial \mathbf{A}}{\partial \rho_k} \Psi_n}{\Phi_n^T \Psi_n} \quad (9)$$

where Φ_n and Ψ_n denote the left and right eigenvectors associated with the n^{th} eigenvalue λ_n of \mathbf{A} , respectively. As the system stability is determined by the real part of eigenvalues, its sensitivity analysis is more of interest. Fig. 10 shows the sensitivity analysis of the real part of critical poles in Fig. 9. The positive sensitivity means that increasing the parameter will move the corresponding pole rightwards. Alternatively, the negative sensitivity suggests that increasing the parameter will move the corresponding pole leftwards. According to Fig. 10, increasing K_f will decrease the real part of the critical poles, as indicated by Fig. 9. The remaining parameters may also be tuned by the sensitivity analysis result.

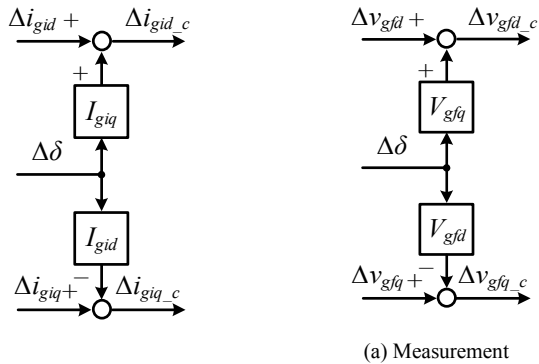


Fig. 8. Linearized frame rotation model.

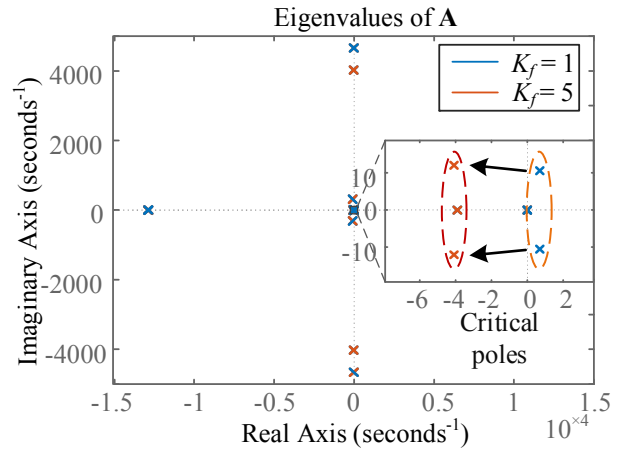


Fig. 9. Eigenvalues of \mathbf{A} when $K_f = 1$ and $K_f = 5$.

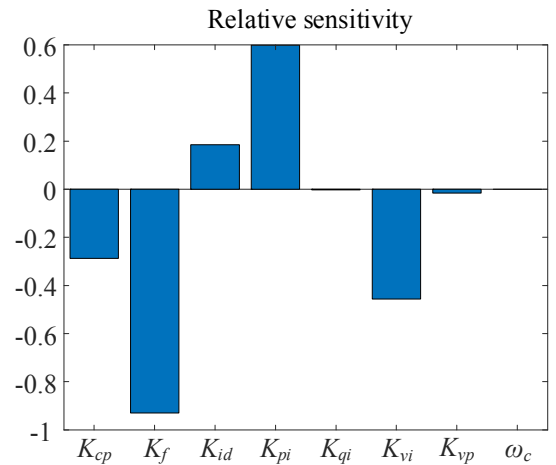
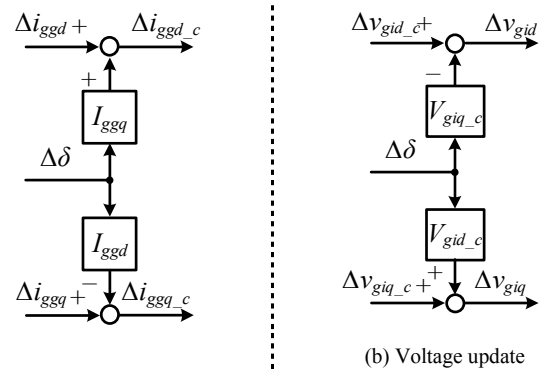


Fig. 10. Sensitivity analysis of critical poles.

IV. SIMULATION AND EXPERIMENTAL RESULTS

Fig. 11 illustrates the active and reactive power responses of the small signal model and the simulation (under the Matlab/Simulink environment) under a 10% active power reference step-up change, where the close resemblance between the two cases can be easily noticed.

Fig. 12 demonstrates the frequency regulation performances, where the inertia emulated by the grid-forming converter is compared with the ideal power system



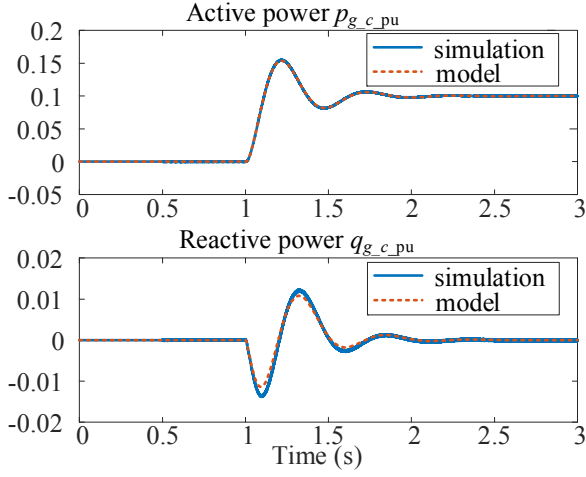


Fig. 11. Active and reactive power responses of small signal model and simulation under a 10% step-up active power reference change.

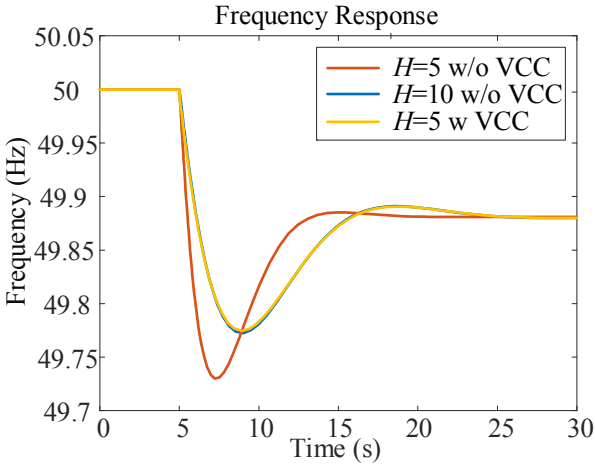


Fig. 12. Frequency responses of the power systems with and without VCC under a 5% step-up load change.

inertia. In the first and second cases, the power systems are operated with the synchronous generator alone, and the relevant inertia constants are $H = 5$ s and $H = 10$ s, respectively. In the third case, the grid-forming power converter featuring an inertia constant H_{VCC} of 5 s is operated in parallel to the synchronous generator with $H = 5$ s. The simulation result indicates that the virtual inertia provided by the grid-forming converter is almost identical to the power system inertia.

Experiments were carried out to further demonstrate the effectiveness of modeling, stability analysis, and stability improvement. The grid forming converter is controlled by the dSPACE (Microlabbox), and the grid is emulated by the Chroma Regenerative Grid Simulator. The system parameters and the control parameters are shown in TABLE I and TABLE II. Before being connected to the grid, the grid-forming power converter synchronizes with the grid through a PLL until there are no phase and voltage amplitude differences.

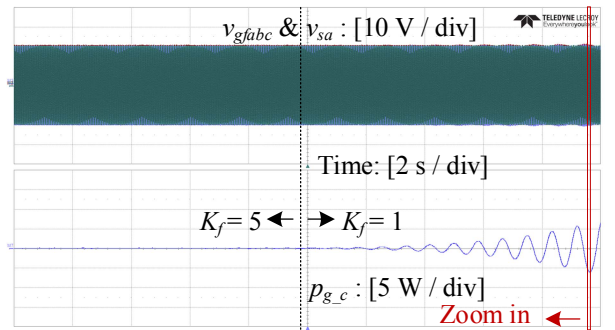
The experimental results shown in Fig. 13 verify the stability enhancement by adding the lead-lag compensator. When K_f changes from 5 to 1, the lead-lag compensator is bypassed. Meanwhile, the output active power p_{g_c} of the

TABLE I. System Parameters.

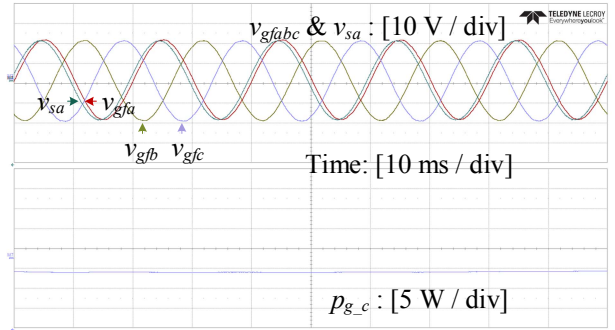
Description	System Parameter	
	Symbol	Value
Nominal frequency	f_n	50 Hz
Nominal phase voltage amplitude	V_n	20 V
Grid phase voltage amplitude	V_s	20 V
LC filter converter side inductance	L_{gi}	2 mH
LC filter capacitance	C_{gf}	40 μ F
Grid resistance	R_s	0 Ω
Grid inductance	L_s	5 mH
DC link voltage	V_{dc}	50 V
Nominal power	P_n	100 W

TABLE II. Control Parameters.

Description	Control Parameter	
	Symbol	Value
Sampling rate	f_n	10 kHz
Inertia constant	H	5 s
Lead-lag compensator cut-off frequency	ω_c	52
Reactive power integral gain	K_{qi}	10
Current controller proportional gain	K_{cp}	0.4
Current controller integral gain	K_{ci}	0
Current controller feedback gain	K_{id}	1.6
Voltage controller proportional gain	K_{vp}	0.2
Voltage controller integral gain	K_{vi}	70



(a) Overall view



(b) Zoom-in view

Fig. 13. Experimental waveforms of the converter output voltages and power with $K_f = 5$ and $K_f = 1$.

grid-forming converter starts to diverge, indicating an unstable system.

V. CONCLUSION AND FUTURE WORK

This paper achieves inertia emulation by using grid-forming power converters. A detailed small-signal model is

built, based on which the stability analysis is carried out. Through the sensitivity analysis, the decisive control parameters are identified. Further, a lead-lag compensator is proposed to stabilize the system. With the proposed control, grid-forming power converters can take over the responsibility of synchronous generators to emulate inertia and form the grid in more-electronics power systems.

The proposed lead-lag compensator can be further applied to the grid-forming converters whose dc source is a variable voltage source, i.e. a capacitor, where the droop control is unable to apply as they are unable to output continuous active power.

APPENDIX A: SMALL SIGNAL STATE-SPACE MODEL

The state matrix \mathbf{A} and the input matrix \mathbf{B} of the state space model (8) is represented as

$$\dot{\mathbf{x}} = [\mathbf{A}_{1-4} \quad \mathbf{A}_{5-12} \quad \mathbf{A}_{13-16}] \mathbf{x} + \mathbf{B} \mathbf{u} \quad (10)$$

The detailed sub-matrices of \mathbf{A} are given by (11) – (13), the matrix \mathbf{B} is given by (14).

REFERENCES

- [1] J. Fang, H. Li, Y. Tang, and F. Blaabjerg, "On the Inertia of Future More-Electronics Power Systems," *IEEE Journal of Emerging and Selected Topics in Power Electronics*, in press.
- [2] J. Rocabert, A. Luna, F. Blaabjerg, and P. Rodríguez, "Control of Power Converters in AC Microgrids," *IEEE Transactions on Power Electronics*, vol. 27, no. 11, pp. 4734-4749, 2012.
- [3] Q. Zhong, P. Nguyen, Z. Ma and W. Sheng, "Self-Synchronized Synchronverters: Inverters Without a Dedicated Synchronization Unit," *IEEE Transactions on Power Electronics*, vol. 29, no. 2, pp. 617-630, Feb. 2014.
- [4] Q. Zhong and G. Weiss, "Synchronverters: Inverters That Mimic Synchronous Generators," *IEEE Transactions on Industrial Electronics*, vol. 58, no. 4, pp. 1259-1267, April 2011.
- [5] H. Wu *et al.*, "Small-Signal Modeling and Parameters Design for Virtual Synchronous Generators," *IEEE Transactions on Industrial Electronics*, vol. 63, no. 7, pp. 4292-4303, 2016.
- [6] O. Mo, S. D'Arco, and J. A. Suul, "Evaluation of Virtual Synchronous Machines With Dynamic or Quasi-Stationary Machine Models," *IEEE Transactions on Industrial Electronics*, vol. 64, no. 7, pp. 5952-5962, 2017.
- [7] P. Kundur, *Power system stability and control*. McGraw-hill New York, 1994.

$$\begin{aligned}
\mathbf{A}_{1-4} = & \\
& \left[\begin{array}{cccc}
0 & 0 & \frac{3(I_{ggd}V_{gfq_c} - I_{ggq}V_{gfd_c} - I_{gdd_c}V_{gfq} + I_{gqq_c}V_{gfd})}{2P_n} & 0 \\
K_{pi} & -\omega_c & \frac{3K_{pp}(I_{ggd}V_{gfq_c} - I_{ggq}V_{gfd_c} - I_{gdd_c}V_{gfq} + I_{gqq_c}V_{gfd})}{2P_n} & 0 \\
K_f K_{pi} \omega_0 & \omega_0(\omega_c - K_f \omega_c) & \frac{3K_{pp}K_f \omega_0(I_{ggd}V_{gfq_c} - I_{ggq}V_{gfd_c} - I_{gdd_c}V_{gfq} + I_{gqq_c}V_{gfd})}{2P_n} & 0 \\
0 & 0 & \frac{3(I_{gdd}V_{gfd_c} + I_{gqq}V_{gfq_c} - I_{gdd_c}V_{gfd} - I_{gqq_c}V_{gfq})}{2P_n} & 0 \\
0 & 0 & -V_{gfq} - \frac{3K_{qp}V_n(I_{ggd}V_{gfd_c} + I_{gqq}V_{gfq_c} - I_{gdd_c}V_{gfd} - I_{gqq_c}V_{gfq})}{2P_n} & K_{qi}V_n \\
0 & 0 & V_{gfd} & 0 \\
0 & 0 & -K_{vp}V_{gfq} - I_{giq}K_{id} - \frac{3K_{qp}K_{vp}V_n(I_{ggd}V_{gfd_c} + I_{gqq}V_{gfq_c} - I_{gdd_c}V_{gfd} - I_{gqq_c}V_{gfq})}{2P_n} & K_{qi}K_{vp}V_n \\
0 & 0 & K_{vp}V_{gfd} + I_{gid}K_{id} & 0 \\
0 & 0 & -\frac{8K_{cp}(K_{vp}V_{gfq} + K_{id}I_{giq})}{3T_s} - \frac{4K_{cp}K_{qp}K_{vp}V_n(I_{ggd}V_{gfd_c} + I_{gqq}V_{gfq_c} - I_{gdd_c}V_{gfd} - I_{gqq_c}V_{gfq})}{P_n T_s} & \frac{8K_{cp}K_{qi}K_{vp}V_n}{3T_s} \\
0 & 0 & \frac{8K_{cp}(K_{vp}V_{gfd} + K_{id}I_{gid})}{3T_s} & 0 \\
0 & 0 & \frac{I_{giq}K_{cp}K_{id} - V_{giq_c} + K_{cp}K_{vp}V_{gfq}}{L_{gi}} + \frac{3K_{cp}K_{qp}K_{vp}V_n(I_{ggd}V_{gfd_c} + I_{gqq}V_{gfq_c} - I_{gdd_c}V_{gfd} - I_{gqq_c}V_{gfq})}{2P_n L_{gi}} & -\frac{K_{cp}K_{qi}K_{vp}V_n}{L_{gi}} \\
0 & 0 & -\frac{I_{gid}K_{cp}K_{id} - V_{gid_c} + K_{cp}K_{vp}V_{gfd}}{L_{gi}} & 0 \\
0 & 0 & 0 & 0 \\
0 & 0 & 0 & 0 \\
0 & 0 & 0 & 0
\end{array} \right] \quad (11)
\end{aligned}$$

$$\begin{aligned}
& \mathbf{A}_{5-12} = \\
& \left[\begin{array}{ccccccc}
0 & 0 & 0 & 0 & 0 & 0 & 0 \\
0 & 0 & 0 & 0 & 0 & 0 & 0 \\
0 & 0 & 0 & 0 & 0 & 0 & 0 \\
0 & 0 & 0 & 0 & 0 & 0 & 0 \\
0 & 0 & 0 & 0 & 0 & 0 & 0 \\
0 & 0 & 0 & 0 & 0 & 0 & 0 \\
0 & 0 & 0 & 0 & 0 & 0 & 0 \\
K_{vi} & 0 & 0 & 0 & 0 & -K_{id} & 0 \\
0 & K_{vi} & 0 & 0 & 0 & 0 & -K_{id} \\
\frac{8K_{cp}K_{vi}}{3T_s} & 0 & \frac{8K_{ci}}{3T_s} & 0 & -\frac{4}{3T_s} & 0 & -\frac{8K_{cp}K_{id}}{3T_s} & 0 \\
0 & \frac{8K_{cp}K_{vi}}{3T_s} & 0 & \frac{8K_{ci}}{3T_s} & 0 & -\frac{4}{3T_s} & 0 & -\frac{8K_{cp}K_{id}}{3T_s} \\
-\frac{K_{cp}K_{vi}}{L_{gi}} & 0 & -\frac{K_{ci}}{L_{gi}} & 0 & \frac{1}{L_{gi}} & 0 & \frac{K_{cp}K_{id}}{L_{gi}} & \omega_0 \\
0 & -\frac{K_{cp}K_{vi}}{L_{gi}} & 0 & -\frac{K_{ci}}{L_{gi}} & 0 & \frac{1}{L_{gi}} & -\omega_0 & \frac{K_{cp}K_{id}}{L_{gi}} \\
0 & 0 & 0 & 0 & 0 & 0 & \frac{1}{C_{gf}} & 0 \\
0 & 0 & 0 & 0 & 0 & 0 & 0 & \frac{1}{C_{gf}} \\
0 & 0 & 0 & 0 & 0 & 0 & 0 & 0 \\
0 & 0 & 0 & 0 & 0 & 0 & 0 & 0
\end{array} \right] \quad (12)
\end{aligned}$$

$$\begin{aligned}
& \mathbf{B} = \\
& \left[\begin{array}{cccc}
1 & 0 & 0 & 0 \\
K_{pp} & 0 & 0 & 0 \\
K_f K_{pp} \omega_0 & 0 & 0 & 0 \\
0 & 1 & 0 & 0 \\
0 & K_{qp} V_n & 0 & 0 \\
0 & 0 & 0 & 0 \\
0 & K_{qp} K_{vp} V_n & 0 & 0 \\
0 & 0 & 0 & 0 \\
0 & \frac{8K_{cp} K_{qp} K_{vp} V_n}{3T_s} & 0 & 0 \\
0 & 0 & 0 & 0 \\
0 & -\frac{K_{cp} K_{qp} K_{vp} V_n}{L_{gi}} & 0 & 0 \\
0 & 0 & 0 & 0 \\
0 & 0 & 0 & 0 \\
0 & 0 & 0 & -\frac{1}{L_{gg} + L_s} \\
0 & 0 & 0 & -\frac{1}{L_{gg} + L_s}
\end{array} \right] \quad (14)
\end{aligned}$$

$$\begin{aligned}
& \mathbf{A}_{13-16} = \\
& \left[\begin{array}{cccc}
-\frac{3I_{gqd_c}}{2P_n} & -\frac{3I_{gqg_c}}{2P_n} & -\frac{3V_{gfd_c}}{2P_n} & -\frac{3V_{gqf_c}}{2P_n} \\
-\frac{3I_{gqd_c} K_{pp}}{2P_n} & -\frac{3I_{gqg_c} K_{pp}}{2P_n} & -\frac{3K_{pp} V_{gfd_c}}{2P_n} & -\frac{3K_{pp} V_{gqf_c}}{2P_n} \\
-\frac{3I_{gqd_c} K_{pp} K_f \omega_0}{2P_n} & -\frac{3I_{gqg_c} K_{pp} K_f \omega_0}{2P_n} & -\frac{3K_{pp} K_f \omega_0 V_{gfd_c}}{2P_n} & -\frac{3K_{pp} K_f \omega_0 V_{gqf_c}}{2P_n} \\
\frac{3I_{gqd_c}}{2P_n} & -\frac{3I_{gqg_c}}{2P_n} & -\frac{3V_{gqf_c}}{2P_n} & \frac{3V_{gfd_c}}{2P_n} \\
\frac{3K_{qp} V_n I_{gqd_c}}{2P_n} - 1 & -\frac{3K_{qp} V_n I_{gqd_c}}{2P_n} & -\frac{3K_{qp} V_n f_{gqf_c} V_n}{2P_n} & \frac{3K_{qp} V_n f_{gfd_c} V_n}{2P_n} \\
0 & -1 & 0 & 0 \\
\frac{3K_{qp} K_{vp} V_n I_{gqd_c}}{2P_n} - K_{vp} & -\frac{3K_{qp} K_{vp} V_n I_{gqd_c}}{2P_n} & -\frac{3K_{qp} K_{vp} V_{gqf_c} V_n}{2P_n} & \frac{3K_{qp} K_{vp} V_{gfd_c} V_n}{2P_n} \\
0 & -K_{vp} & 0 & 0 \\
\frac{4I_{gqg_c} K_{cp} K_{qp} K_{vp} V_n}{P_n T_s} - \frac{8K_{cp} K_{vp}}{3T_s} & -\frac{4I_{gqd_c} K_{cp} K_{qp} K_{vp} V_n}{P_n T_s} & -\frac{4K_{cp} K_{qp} K_{vp} V_{gqf_c} V_n}{P_n T_s} & \frac{4K_{cp} K_{qp} K_{vp} V_{gfd_c} V_n}{P_n T_s} \\
0 & -\frac{8K_{cp} K_{vp}}{3T_s} & 0 & 0 \\
K_{cp} K_{vp} - 1 & -\frac{3I_{gqd_c} K_{cp} K_{qp} K_{vp} V_n}{2P_n L_{gi}} & \frac{3I_{gqd_c} K_{cp} K_{qp} K_{vp} V_n}{2P_n L_{gi}} & \frac{3K_{cp} K_{qp} K_{vp} V_{gqf_c} V_n}{2P_n L_{gi}} \\
& 0 & \frac{K_{cp} K_{vp} - 1}{L_{gi}} & 0 \\
0 & \omega_0 & -\frac{1}{C_{gf}} & 0 \\
-\omega_0 & 0 & 0 & -\frac{1}{C_{gf}} \\
\frac{1}{L_{gg} + L_s} & 0 & 0 & \omega_0 \\
0 & \frac{1}{L_{gg} + L_s} & -\omega_0 & 0
\end{array} \right] \quad (13)
\end{aligned}$$